Macromolecules

ARTICLE

pubs.acs.org/Macromolecules

Entanglement Dynamics in Miscible Polyisoprene/Poly(*p-tert*-butylstyrene) Blends

Hiroshi Watanabe,* Quan Chen, Yohji Kawasaki, and Yumi Matsumiya

Institute for Chemical Research, Kyoto University, Uji, Kyoto 611-0011, Japan

Tadashi Inoue and Osamu Urakawa

Department of Macromolecular Science, Faculty of Science, Osaka University, Toyonaka, Osaka 560-0043, Japan

ABSTRACT: Viscoelastic, dielectric, and rheo-optical behavior was examined for miscible blends of high-*M cis*-polyisoprene (PI) and poly(*p-tert*-butylstyrene) (PtBS). The slow dielectric relaxation of the blends was exclusively attributed to the global motion of the PI chains having the type-A dipoles. The PI and PtBS chains behaved as the fast and slow (low- and high-friction) components and were well entangled with each other. The dynamics of these chains changed significantly with temperature T. At high T, the blend exhibited two-step entanglement plateau of the storage modulus $G'(\omega)$, and the plateaus at high and low angular frequencies (ω) were attributed, with the aid of the dielectric data, to the entanglement among all component chains and that between the PtBS chains, respectively. The entanglement length a characterizing the high-ω plateau was well described by a simple mixing rule based on the number fraction n of the Kuhn segments of the components, $a = n_{PI}a_{PI}^{bulk} + n_{PtBS}a_{PtBS}^{bulk}$. This result was consistent with the current molecular picture relating the entanglement density to the packing length p ($\cong a/20$). The complex moduli G^* of the blends in the high-ω plateau zone were well described by a simple blending law combined with this mixing rule of a, which was consistent with the rheo-optical data. At low T, the blend exhibited the Rouse-like power-law behavior of storage and loss moduli, $G' = G'' \propto \omega^{1/2}$, in the range of ω where the high-ω plateau was supposed to emerge. This lack of the high-ω plateau was attributed to retardation of the Rouse equilibration of the PI chain over the entanglement length a due to the hindrance from the slow PtBS chains: The PI and PtBS chains appeared to be equilibrated *cooperatively/simultaneously* at a rate essentially determined by PtBS. The Rouse equilibration time, evaluated from the G^* data of the blend, was just moderately shorter than the dielectrically determined relaxation time of PI. Thus, the high-ω plateau zone was too narrow to be resolved experimentally, and the PI chains relaxed almost immediately after their Rouse equilibration (retarded by PtBS). This PI relaxation activated the constraint release (CR) relaxation of PtBS to dilate the entanglement mesh for PtBS. A simple model considering the Rouse equilibration and CR/dilation processes described the G^* data of the blend surprisingly well, lending support to the molecular picture of the cooperative/simultaneous Rouse equilibration of the PI and PtBS chains. The model calculation was consistent with the rheo-optical data, which lent further support to this molecular picture.

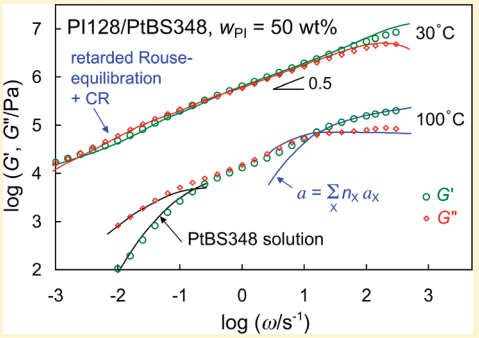

1. INTRODUCTION

The entanglement dynamics of long flexible polymer chains is one of the central research subjects in the field of polymer physics. For homopolymer systems, this dynamics has been extensively investigated from experimental and theoretical aspects to reveal some specific mechanisms that govern the global relaxation of the chain. For example, within the content of the tube model, the terminal viscoelastic relaxation of linear chains is activated mainly by the reptation mechanism and accelerated/broadened by the contour length fluctuation (CLF) and constraint release (CR) mechanisms.[1−5] In particular, the CR mechanism is essential in binary blends of chains having widely separated molecular weights (M).[2,3] Similar effects are naturally expected for miscible blends of chemically different chains. However, an interesting and important difference is noted between the blends of chemically identical chains (homopolymer systems) and of chemically different chains. Namely, the local segmental friction ζ_s and the entanglement molecular weight M_e, the basic parameters affecting the entanglement relaxation, are common for all component chains in the former type of blends but not in the latter. Thus, it is very interesting to examine ζ_s and M_e in the miscible blends of chemically different chains.

For such miscible blends of two components, say A and B, dynamics of the monomeric segments has been extensively investigated in relation to the concepts of the self-concentration[6] and the local composition fluctuation.[7] The motion of a given A segment is strongly affected by the surrounding segments that include the chemically different B segments. When the component B has a bulk glass transition temperature $T_{g,B}^{bulk}$ much

Received: November 15, 2010
Revised: January 18, 2011
Published: February 18, 2011

higher than $T_{g,A}^{bulk}$ of the component A, the two components do not necessarily have the same effective T_g^{eff} but often exhibit $T_{g,B}^{eff} > T_{g,A}^{eff}$ in the miscible blends. This difference of T_g^{eff} is attributable to a difference of the intrachain torsional barriers of the components A and B and, more importantly, to the self-concentration,[6] i.e., enrichment of the segments A (or B) around a given segment A (B) due to the chain connectivity. The difference of the local compositions around the segments A and B due to the self-concentration results in slower segmental motion of B compared to A that can be represented as a difference of the segmental frictions, $\zeta_{s,B} > \zeta_{s,A}$. (The temperature ($T$) dependence of ζ_s is basically described by the WLF equation with respect to T_g^{eff} so that $\zeta_{s,B} > \zeta_{s,A}$ for the case of $T_{g,B}^{eff} > T_{g,A}^{eff}$ and the difference between $\zeta_{s,B}$ and $\zeta_{s,A}$ is enhanced at low T.) Furthermore, this local composition is not the same for all A (or B) segments but dynamically fluctuates with time. Thus, in the time scale of the segmental motion where this fluctuation has not been equilibrated, $\zeta_{s,X}$ has a distribution among the segments X (=A, B)[7] with its mean value $\overline{\zeta}_{s,X}$ being determined by the macroscopic (average) composition and the self-concentration. Characteristic features of the segmental dynamics in the miscible blends,[6−23] broad glass transition observed through thermal measurements, broad spectra of segmental dynamics detected with NMR, and the broad and thermo-rheologically complex dielectric/viscoelastic segmental relaxation processes are rather well understood in relation to the self-concentration and dynamic fluctuation effects.

The global, entanglement dynamics in miscible blends has been also investigated[22,24−29] but less clearly understood compared to the local segmental dynamics. These blends often exhibit two-step entanglement relaxation qualitatively similar to that observed for binary blends of chemically identical chains. However, the temperature dependence of ζ_s is different for the two components in the miscible blends (because of the difference of their T_g^{eff}), which results in the thermo-rheological complexity of the entanglement relaxation of these blends. This complexity has been incorporated in the tube model (originally developed for chemically uniform systems) to reformulate the model for the miscible blends on the basis of the molecular picture of double reptation[26] and dynamic tube dilation.[29] The reformulated models semiquantitatively describe the slow viscoelastic relaxation of miscible blends such as *cis*-polyisoprene (PI)/poly(vinyl ethylene) (PVE) blends. However, no full agreement was found between the model and the data, quite possibly because the double reptation/tube dilation formulations utilized in the models do *not* accurately apply even to chemically uniform homopolymer systems.[23,30−34] (For chemically uniform binary blends of long and short chains, the double reptation/tube dilation molecular pictures are valid only when the length and time scales involved in these pictures are consistently coarse-grained on the basis of the Rouse-CR process of the whole sequence of short−long entanglements.[30−32,34])

Here, it should be noted that the above models for the miscible blends include the entanglement length a (or the entanglement molecular weight $M_e \propto a^2$) as a parameter determining the entanglement plateau modulus G_N as well as the component relaxation times. The comparison of the model prediction and data were based on the a (or M_e) value estimated from a mixing rule(s), for example, $1/a = \phi_A/a_A^{bulk} + \phi_B/a_B^{bulk}$ where a_X^{bulk} is the entanglement length of the component X (X = A, B) in bulk and ϕ_X is the volume fraction of this component in the blend.[26] Since a_X^{bulk} is not significantly different for the components so far examined (*e.g.*, PI and PVE), the other choices of the mixing rule would have given nearly the same a (or M_e) value in the blend and thus have hardly affected the model predictions. Nevertheless, the mixing rule of a (or M_e) should directly reflect the molecular origin of the entanglement intimately related to the packing length. Thus, it is highly desired to distinguish several mixing rules and specify the most appropriate rule.

Table 1. Characteristics of Samples

sample code	$10^{-3}M_w$	M_w/M_n
PtBS348	348	1.06
PI99	98.5	1.04
PI128	128	1.03

In relation to this distinction, we note that PI and poly(*p-tert*-butylstyrene) (PtBS) are miscible in a wide range of temperature[35−38] and have quite different a_X^{bulk} and M_e^{bulk} values in bulk:[39]

$$\text{bulk PI: } a_{PI}^{bulk} = 5.8 \text{ nm}, \quad M_e^{bulk\ PI} = 5.0 \times 10^3 \qquad (1)$$

$$\text{bulk PtBS: } a_{PtBS}^{bulk} = 11.7 \text{ nm}, \quad M_e^{bulk\ PtBS} = 37.6 \times 10^3 \qquad (2)$$

(The M_e values shown in eqs 1 and 2 were evaluated from the G_N data through a relationship, $G_N = \rho RT/M_e$, with ρ, R, and T being the bulk density, gas constant, and absolute temperature, respectively.) Different mixing rules give considerably different a (or M_e) values for the PI/PtBS blends, which enables us to specify the most appropriate rule. Furthermore, PI has the type-A dipole parallel along the chain backbone and its global motion activates dielectric relaxation,[2,40] while PtBS has no type-A dipole and its global motion is dielectrically inert.[36−38] This difference enables us to utilize the dielectric data of PI/PtBS blends to unequivocally determine the terminal relaxation time τ_ε^{PI} of the PI chains therein.[36−38] The viscoelastic modulus of PI in the blend, evaluated from the τ_ε^{PI} data and modulus data of bulk PI, is helpful for accurately specifying the most appropriate mixing rule of a.

Thus, we chose the blends of high-M PI and PtBS as a model system to conduct viscoelastic, dielectric, and rheo-optical measurements. At all temperatures examined, the blends were in the miscible state and the PI and PtBS chains therein behaved as the fast and slow (low-ζ_s and high-ζ_s) components. The viscoelastic, dielectric, and rheo-optical data revealed that the blends exhibit two-step entanglement relaxation at high T and the high frequency (ω) plateau of the modulus at $\omega > 1/\tau_\varepsilon^{PI}$, being sustained by both PI and PtBS, is most appropriately described by a simple mixing rule of a based on the number fraction of the Kuhn segments of PI and PtBS. The data also suggested that the Rouse equilibration of PI at length scales $\leq a$ is significantly retarded by PtBS at low T thereby narrowing the high-ω plateau zone to an undetectable width (and forcing this zone to almost merge with the retarded Rouse relaxation zone). This paper presents details of these results, placing its emphasis on the fundamental aspects of polymer rheology, i.e., the role of the Rouse equilibration in determining the stress and the necessity of this equilibration for appearance of the entanglement plateau.

2. EXPERIMENTAL SECTION

2.1. Materials. A linear high-M PtBS348 sample, previously synthesized anionically,[41] was utilized as the slow component in the PI/PtBS blends. Its characteristics are summarized in Table 1.

Linear high-M PI samples, PI99 and PI128, were anionically synthesized in vacuum at 30 °C utilizing benzene and *sec*-butyllithium as the solvent and initiator, respectively. These samples were characterized

with GPC (CO-8020 and DP-8020, Tosoh) equipped with a refractive index (RI)/low-angle light scattering (LALS) monitor (LS-8000, Tosoh Co). Previously synthesized monodisperse PI samples[36−38,42] were utilized as the LALS and elution standards. The characteristics of the PI99 and PI128 samples are also shown in Table 1. The microstructure determined from ^{1}H NMR (Varian MERCURYplus AS400) were the same for these samples, 1,4-*cis*:1,4-*trans*:3,4 = 78:14:8. This microstructure, very close to that of the previously utilized PI20 (1,4-*cis*:1,4-*trans*:3,4 = 79:14:7),[38] allowed the PI99 and PI128 chains to be miscible with the PtBS348 chain in the entire range of T examined ($T \leq 120$ °C).

The materials subjected to viscoelastic, dielectric, and rheo-optical measurements were the blends of PtBS348 with PI99 and PI128. The blends were prepared according to the previously reported method:[35,38] The prescribed masses of the PtBS and PI samples were dissolved in tetrahydrofuran (THF) at a total concentration of 10 wt % and then precipitated in a dropwise way into an excess methanol/acetone (8/2 wt/wt) mixture vigorously stirred by a magnetic bar. The blends were recovered via decantation and thoroughly dried under vacuum first at room temperature and then at 145 °C. The blends thus prepared were transparent, which is in accord with the PI/PtBS miscibility.

2.2. Measurements. Linear viscoelastic, dielectric, and rheo-optical measurements were conducted for the PI99/PtBS348 and PI128/PtBS348 blends having the PI content of w_{PI} = 40, 50, and 56 wt %. For comparison, the viscoelastic and dielectric measurements were conducted also for respective components in bulk state. The component data are summarized in Appendix A.

The linear viscoelastic measurements were conducted with a laboratory rheometer (ARES, TA Instruments) at several temperatures $T \leq$ 120 °C. Parallel-plate fixtures with diameters of 8 and/or 4 mm were utilized. The oscillatory strain amplitude was kept small ($\gamma_0 \leq 0.1$) to ensure the linearity of the storage and loss moduli, G' and G''. The viscoelastic measurement was conducted also for a 46.7 wt % solution of PtBS348 in a low-M solvent, dibutyl phthalate (DBP). This solution was utilized as a reference system for the 50 wt % PI/PtBS348 blends.

The dielectric measurements (in the linear response regime) were conducted also at $T \leq 120$ °C. The samples were charged in a dielectric cell composed of parallel plate electrodes and a guard electrode. The measurements were made with an impedance analyzer/dielectric interface system (1260 and 1296, Solartron). In this paper, the dielectric data are presented as plots against the angular frequency, $\omega = 2\pi f$ with f being the frequency in hertz units.

Preliminary rheo-optical (dynamic birefringence) measurements were conducted for the 50 wt % PI128/PtBS348 blend at $T \leq 100$ °C with a homemade device composed of an oscillating drive and optical/mechanical detectors.[43] The amplitude of the oscillatory strain was kept small ($\gamma_0 = 0.06$) to ensure the linearity. The dynamic birefringence data were normalized by this amplitude to give the complex shear optical coefficient K^*, and analysis[44−46] of the K^* and the complex modulus G^* ($=G' + iG''$) data enabled us to evaluate the component moduli in the blend.

3. RESULTS AND DISCUSSION

3.1. Overview. For the PI99/PtBS348 blend with w_{PI} = 50 wt %, Figure 1 shows the angular frequency (ω) dependence of the storage and loss moduli, G' and G'', and the dielectric loss, ε'', at temperatures T as indicated. For clarity of the plots, only the data at representative T are shown. The blend was miscible at all T examined. The raw ε'' data are multiplied by a factor of 10^4 and shown in a range of ω where the direct current (dc) conduction negligibly contributes to the data, as done in the previous work.[38] The component molecular weights are significantly larger than M_e^{bulk} in respective bulk systems (cf. eqs 1 and 2), which allows

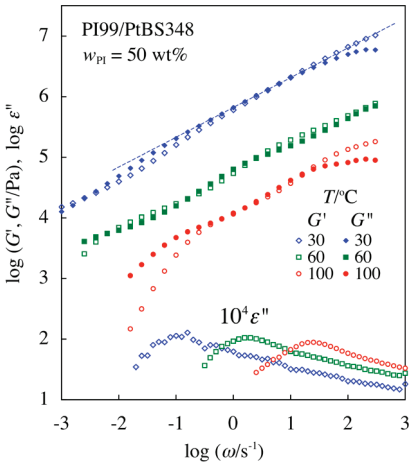

Figure 1. Viscoelastic and dielectric behavior of PI99/PtBS348 blend with w_{PI} = 50 wt % at temperatures as indicated. The ε'' data shown are the raw data without the dc correction. The dotted line attached to the modulus data at 30 °C indicates the Rouse-like power-law behavior, $G' = G'' \propto \omega^{1/2}$.

the PI and PtBS chains to be well entangled in the blend. Since PI has the type-A dipoles while PtBS does not, the dielectric relaxation seen in Figure 1 is exclusively attributed to the global motion (end-to-end vector fluctuation) of the PI chains in the blend. At all T examined, the blends exhibit two-step viscoelastic relaxation and the terminal (second step) relaxation is much slower than the dielectric relaxation. Thus, PI99 and PtBS348 are unequivocally assigned as the fast and slow components in the blends, and the terminal viscoelastic relaxation is attributed to the global motion of the PtBS chains.

The two-step viscoelastic relaxation behavior (Figure 1) was noted for all PI/PtBS blends examined. This behavior is qualitatively similar to that seen for chemically uniform binary blends such as PI/PI blends.[30,31] However, we should also note an important difference, the thermo-rheological complexity of the viscoelastic data of the PI/PtBS blend. This complexity is demonstrated in Figure 2, where we have chosen a reference temperature T_r = 303 K (30 °C), corrected the modulus data with the intensity factor $b_T = T/T_r$, and shifted the corrected $b_T^{-1}G'$ and $b_T^{-1}G''$ data along the ω axis to achieve the best superposition of the $b_T^{-1}G''$ data at $\omega a_T \cong 10^{-3}$ s^{-1}. (For clarity of the plots, the $b_T^{-1}G''$ data are multiplied by a factor of $10^{-1.5}$.) For comparison, the dielectric $b_T\varepsilon''$ data corrected with the intensity factor b_T are multiplied by a factor of 10^4 and shifted *independently* from the modulus data to achieve the best superposition at the ε'' peak. The shift factors for the viscoelastic and dielectric data, $a_{T,G}$ and $a_{T,\varepsilon}$, were quite different, as shown in the inset. This difference naturally emerged because the $a_{T,G}$ data obtained for the low-ω G'' data reflect the dynamics of PtBS (slow component) while the $a_{T,\varepsilon}$ data reflect the dynamics of PI (fast component). Because of the difference between $a_{T,G}$ and $a_{T,\varepsilon}$, we should not directly compare the viscoelastic and dielectric data in Figure 2 (except the data at $T = T_r = 30$ °C).

The thermo-rheological complexity of the modulus data (failure of the superposition) seen in Figure 2 is partly attributed to a fact that PI and PtBS contributing to the modulus have different T dependence of the friction coefficient of their Rouse segments (=smallest motional unit for the rubbery relaxation), $\zeta_{s,PI}$ and $\zeta_{s,PtBS}$: The coefficient $\zeta_{s,PtBS}$ decreases with increasing T much more strongly compared to $\zeta_{s,PI}$.[38] More importantly,

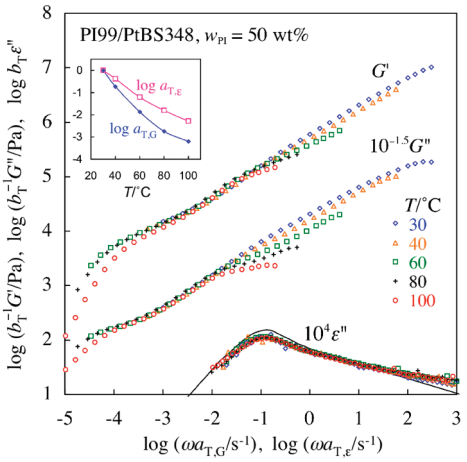

Figure 2. Test of time−temperature superposition for the PI99/PtBS348 blend with w_{PI} = 50 wt %. The solid curve shows the ε'' data of bulk PI99 corrected for the temperature and the PI volume fraction in the blend. For further details, see text.

the complexity results from a significant change of the viscoelastic mode distribution with T: The blend at high T (100 °C) exhibits a plateau of G' and a peak of G'' at high $\omega > 20$ s^{-1} where the terminal relaxation process of PI is dielectrically detected, while the blend at low T (30 °C) shows neither G'-plateau nor G''-peak in the PI relaxation zone at $\omega > 0.1$ s^{-1}. Instead, the G' and G'' data at low T exhibit the Rouse-type power-law behavior, $G' = G'' \propto \omega^{1/2}$ (shown with the dotted line in Figure 1), and monotonically increase beyond the levels of G'-plateau/G''-peak seen at high T. Similar behavior was observed for all PI/PtBS blends examined.

The above results strongly suggest that the relaxation mechanism and the corresponding viscoelastic mode distribution of the PI/PtBS blends change with T and this change governs the thermo-rheological complexity of the blend. In relation to this point, we note that the two-step plateau of G' and the corresponding double peak/shoulder of G'' seen for the blend at high T (Figure 1) are very similar to those of the chemically uniform binary blends[30,31] (reflecting the reptation/CLF mechanism combined with the CR/tube dilation mechanism). Thus, the PI/PtBS blends at high T appear to serve as the good model system for our test of the mixing rule of the entanglement length a. In the next section, we utilize the G' and G'' data of those blends at high ω to achieve this test. The rheo-optical data are also utilized to check the results of the test.

After this test, we examine a change of the relaxation mechanism(s) in the PI/PtBS blends on the decrease of T and discuss why the high-ω Rouse-like behavior is observed at low T instead of the plateau and peak of G' and G'' (cf. Figure 1). In relation to this discussion, we note in Figure 2 that the time−temperature superposition satisfactorily works for the ε'' data of PI in the blend despite the failure of the superposition for the G* data and that the shift factor is quite different for ε'' data and low-ω G'' data (i.e., for the PI and PtBS chains). Furthermore, the superposed ε'' data are close to the data of bulk PI corrected for the temperature and the PI volume fraction in the blend (solid curve), as explained later in more detail. Thus, the relaxation mechanisms of PI at high and low T are different but should be still associated with the same dielectric mode distribution, which provides us with a clue for specifying those mechanisms.

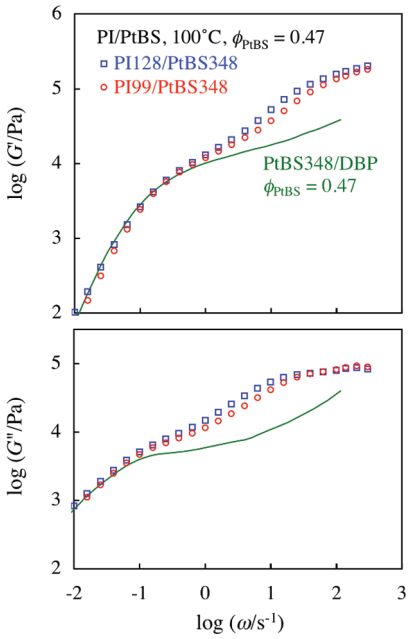

Figure 3. Comparison of the viscoelastic behavior of PI99/PtBS348 and PI128/PtBS348 blends with that of a PtBS/DBP solution. All systems have the same PtBS volume fraction, ϕ_{PtBS} = 0.47. For further details, see text.

3.2. Mixing Rule of Entanglement Length. *3.2.1. Test for Viscoelastic Modulus Data.* The test of the mixing rule of the entanglement length a can be made unequivocally for the PI/PtBS blends at high T if the behavior of those blends is similar to that of the chemically uniform blends (such as PI/PI blends[30,31]). It is well-known that the chemically uniform blends have the entanglement plateau G_N being independent of the component molecular weights M and volume fraction ϕ and that the relaxation behavior of the slow component therein is insensitive to M_{fast} of the fast component and close to the behavior in the solution having the same ϕ_{slow} if the fast and slow components have widely separated relaxation times. We examined these features for the 50 wt % PI99/PtBS348 and PI128/PtBS348 blends (ϕ_{PtBS} = 0.47 as evaluated under the assumption of volume additivity) at 100 °C and the 46.7 wt % PtBS348/DBP solution having the same ϕ_{PtBS}. The results are shown in Figure 3. The solution data at 20 °C corrected for the intensity factor b_T (= T/T_r = 293/373), $b_T^{-1}G_{sol}$*, were shifted along the ω axis to match the viscosity with that of the blends. Clearly, the data of the blends in the low-ω plateau zone are insensitive to M_{PI} of PI (fast component) and agree well with the solution data. Furthermore, G_N of the blends in the high-ω plateau zone is insensitive to M_{PI} and the relaxation from this plateau is slower for larger M_{PI}. All these features are very similar to those of the chemically uniform blends, confirming that the PI/PtBS blends at high T do serve as the good model system for the test of the mixing rule of a.

Now, we test the empirical mixing rules of the entanglement length a proposed in the literature

$$\frac{1}{a} = \frac{\phi_A}{a_A^{bulk}} + \frac{\phi_B}{a_B^{bulk}} \qquad \text{(ref 26)} \qquad (3)$$

and

$$a = n_A a_A^{bulk} + n_B a_B^{bulk} \qquad \text{(ref 38)} \qquad (4)$$

dx.doi.org/10.1021/ma102596b |*Macromolecules* 2011, 44, 1570–1584

a_X^{bulk} denotes the entanglement length in the bulk system of the component X (= A, B), and n_X is the number fraction of the Kuhn segments of the component X in the blend. (eq 4 was originally formulated for the packing length $p \cong a/20$.[38] However, in this study, we neglect a small variation in the p/a ratio among polymer species and utilize eq 4 rewritten for a.) Note also that the mixing rules, eqs 3 and 4, are based on a molecular picture that the high-ω plateau is sustained by both A and B (PI and PtBS) chains and these chains are cooperatively/simultaneously equilibrated to have the same a value. This molecular scenario sounds very reasonable, although we cannot fully rule out the other possibility that the component chains are separately equilibrated to have different a values and different thermal tensions ($=3k_BT/a$). This possibility is discussed in a later section in more detail.

A mixing rule for the entanglement molecular weight M_e, similar but not identical to eq 3, has also been proposed in the literature:[29]

$$\frac{1}{M_e^{1/2}} = \frac{\phi_A}{\{M_e^{bulk\ A}\}^{1/2}} + \frac{\phi_B}{\{M_e^{bulk\ B}\}^{1/2}} \quad (5)$$

In the following, we also test this mixing rule.

We can test eqs 3−5 on the basis of a formal blending law of the complex modulus, $G^*(\omega) = \Sigma_{X=A,B}\, G_X^{bld*}(\omega)$ with $G_X^{bld*}(\omega)$ being the complex modulus of the component X *in the blend*. In general, $G_X^{bld*}(\omega)$ does not coincide with $G_X^{bulk*}(\omega)$ of bulk component X because of the CR effect on $G_X^{bld*}(\omega)$, and this formal blending law merely represents the stress additivity of the components. Nevertheless, in the high-ω plateau zone where eqs 3−5 are to be tested, the fast component has hardly relaxed, thereby activating *no* significant CR relaxation for the fast and slow components. In this zone, G_X^{bld*} at a given T can be approximated to have the same relaxation mode distribution as the bulk modulus G_X^{bulk*} at the same T, as suggested from the G^* data of PI/PI and PS/PS blends in the high-ω plateau zone (cf. Figure 15 of ref 38 and Figure 26 of ref 2). Then, the above blending law can be cast in a form,

$$G^*(\omega) = \sum_{X=A,\,B} \phi_X I_X G_X^{bulk*}(\omega\lambda_X) \text{ in the high-}\omega\text{plateau zone} \quad (6)$$

with

$$\lambda_X = \frac{\tau_G^X}{\tau_G^{bulk\ X}} \quad (7)$$

and

$$I_X = \left(\frac{a_X^{bulk}}{a}\right)^2 \text{ (when eqs 3 and 4 are utilized)} \quad (8a)$$

$$I_X = \frac{M_e^{bulk\ X}}{M_e} \text{ (when eq 5 is utilized)} \quad (8b)$$

Here, λ_X denotes a difference of the viscoelastic relaxation times of the component X in bulk ($\tau_G^{bulk\ X}$) and in the blend (τ_G^X), and I_X represents a difference of the entanglement plateau heights normalized to unit volume fraction of the component X in bulk and blend. I_X is determined according to the mixing rules, eqs 3−5.

A comment needs to be added for λ_X. The PI chains (fast component) in our PI/PtBS blends exhibit a narrow dielectric mode distribution so that their terminal dielectric relaxation time τ_ε^{PI} can be experimentally determined from the angular frequency ω_{peak} for the ε'' peak as $\tau_\varepsilon^{PI} = 1/\omega_{peak}$ (=0.04 s at 100 °C); cf. Figure 1. Since the PI chains relax much faster than the PtBS chains, the entanglement constraint from the PtBS chains is effective throughout the terminal relaxation of the PI chains. For this case, we can safely replace the viscoelastic τ_G^{PI} of PI in the blend by the dielectric τ_ε^{PI} and experimentally evaluate λ_{PI} from the data of τ_ε^{PI} and $\tau_G^{bulk\ PI}$ (= 0.2 s at 30 °C; obtained from the G_{PI}^{bulk*} shown in Appendix A) as $\lambda_{PI} = \tau_\varepsilon^{PI}/\tau_G^{bulk\ PI}$.[47] Indeed, from the previously reported empirical equation for τ_G^{PI} of the fast component,[38] the difference between τ_G^{PI} and τ_ε^{PI} for our PI/PtBS blends was estimated to be less than 5% and can be safely neglected. We also note that the first step relaxation of the slow PtBS chains is activated by the terminal relaxation of PI (through the CR mechanism). Thus, τ_G^{PtBS} of PtBS appearing in eq 7 can be safely replaced by τ_G^{PI} ($=\tau_\varepsilon^{PI}$) of PI, as suggested from the G'' and ε'' data of PI/PI blends in the high-ω plateau zone (cf. Figures 15 and 16 of ref 38). Then, λ_{PtBS} is evaluated from τ_ε^{PI} and the $\tau_G^{bulk\ PtBS}$ data of bulk PtBS as $\lambda_{PtBS} = \tau_\varepsilon^{PI}/\tau_G^{bulk\ PtBS}$.

Utilizing the G_{PI}^{bulk*} and G_{PtBS}^{bulk*} data shown in Appendix A and the λ_{PI} and λ_{PtBS} values obtained above, we calculated the modulus $G^*(\omega)$ of the blend (eq 6) expected for respective mixing rules, eqs 3−5. For the PI/PtBS blends examined, Figures 4− 7 compare the calculated G^* (solid curves) with the G^* data (circles) at high T. The PI and PtBS chains hardly exhibit the entanglement relaxation at ω well above a characteristic frequency ω_x where the plots of the G' and G'' data cross with each other ($\omega_x = 10\ s^{-1}$ in Figure 4, for example). The mixing rules are to be tested in the entanglement plateau zone at $\omega > \omega_x$. Clearly, eqs 3 and 5 (curves in panels a and c) considerably underestimate the modulus in this zone, i.e., overestimate

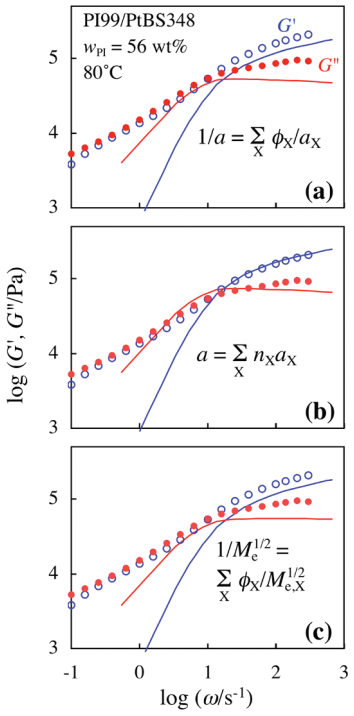

Figure 4. Comparison of the G^* data of PI99/PtBS348 blend (w_{PI} = 56 wt %) at 80 °C with the prediction of eqs 3−5 combined with eq 6.

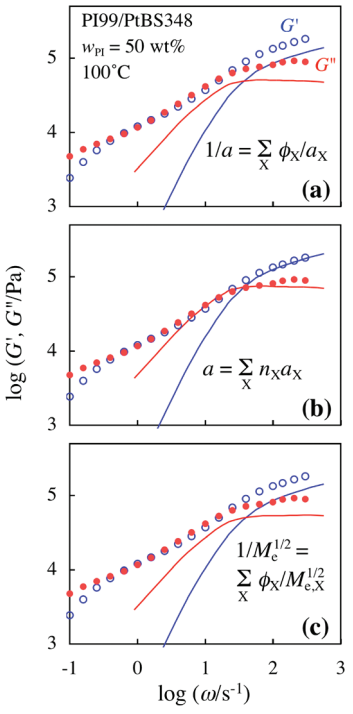

Figure 5. Comparison of the G^* data of PI99/PtBS348 blend (w_{PI} = 50 wt %) at 100 °C with the prediction of eqs 3−5 combined with eq 6.

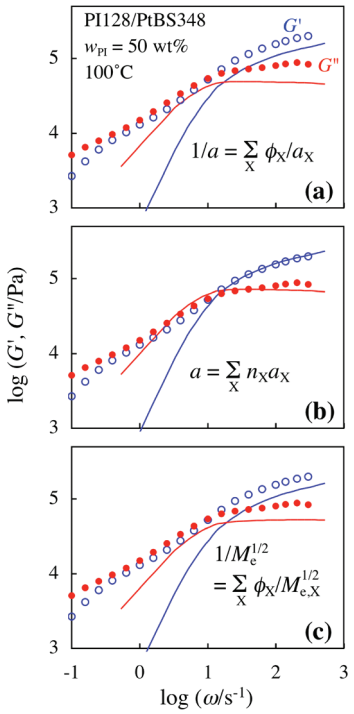

Figure 6. Comparison of the G^* data of PI128/PtBS348 blend (w_{PI} = 50 wt %) at 100 °C with the prediction of eqs 3−5 combined with eq 6.

a and/or M_e in the blends. In contrast, eq 4 (curves in panel b) well describes the G^* data in the high-ω plateau zone where eq 4 is to apply. Note also that the difference of G^* predicted from eq 4 and from eqs 3 and 5 becomes larger with decreasing w_{PI} (because n_{PI} appearing in eq 4 decreases rather weakly with decreasing w_{PI}.)

Here, a comment needs to be added for the validity of eq 4. In the current molecular picture, the entanglement density in homopolymer systems is related to the packing length p, and p is proportional to the entanglement length a ($p \cong a/20$).[39,48,49] Thus, in the PI/PtBS blend, the high-ω plateau is naturally determined by an average of a_{PI}^{bulk} and a_{PtBS}^{bulk}. The Kuhn segment is the fundamental unit for description of the flexible polymer conformation so that the average should include the number fractions of these segments as the weighing factors, which results in the mixing rule given by eq 4. The molecular weight of the Kuhn segment M_{Kuhn} is considerably larger for PtBS ($M_{Kuhn} \cong 1500$)[50] than for PI ($M_{Kuhn} \cong 130$)[39] to give $n_{PtBS} \ll n_{PI}$ so that the a value for the PI/PtBS blends obtained from eq 4, a = 6.2, 6.3, and 6.5 nm for w_{PI} = 56, 50, and 40 wt %, is much smaller than the a_{PtBS}^{bulk} value of bulk PtBS (11.7 nm) and close to a_{PI}^{bulk} of bulk PI (5.8 nm). Such small a values are necessary to reproduce the high-ω plateau level seen for the PI/PtBS blends.

It should be also noted that we were able to distinguish eq 4 from the other mixing rules, eqs 3 and 5, because PI and PtBS have quite different a^{bulk} values. For the other pairs of components such as PI and poly(vinyl ethylene), the difference of a^{bulk} is much smaller and all blending rules give nearly the same a (or M_e). In other words, the validity of eq 4 confirmed in this study does not significantly change the results of the previous studies based on eqs 3 and 5. Nevertheless, we should note that eq 4 is most straightforwardly related to the molecular picture of the entanglement based on the packing length concept, which in turn indicates the physical soundness of eq 4.

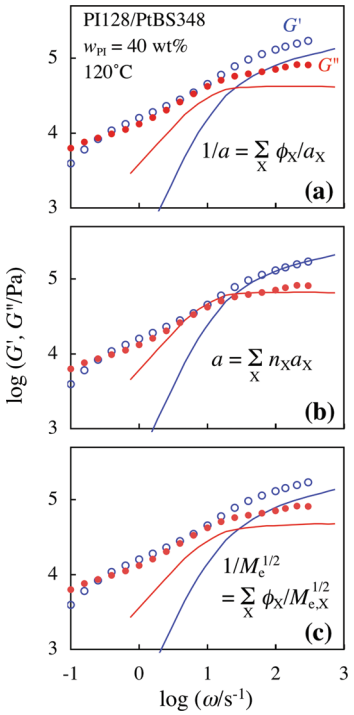

Figure 7. Comparison of the G^* data of PI128/PtBS348 blend (w_{PI} = 40 wt %) at 120 °C with the prediction of eqs 3−5 combined with eq 6.

3.2.2. Test for Preliminary Rheo-Optical Data. We made preliminary rheo-optical measurements to further examine the validity of eq 4. Since the glassy (segmental) relaxation of the

dx.doi.org/10.1021/ma102596b |*Macromolecules* 2011, 44, 1570–1584

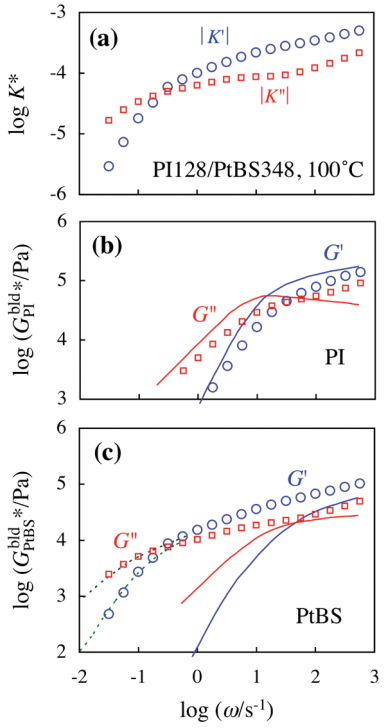

Figure 8. (a) Complex shear optical coefficient of PI128/PtBS348 blend (w_{PI} = 50 wt %) at 100 °C. (b and c) Comparison of the rheo-optically determined component moduli (symbols) with the moduli obtained on the basis of the blending rule, eq 6 combined with eq 4 (solid curves). The dotted curves in part c indicate the G^* data of the blend.

PtBS and PI in the blend at 100 °C occurs at high ω ($\gg 10^4$ s^{-1}), we can neglect the contribution of this relaxation to the complex modulus G^* and the complex shear optical coefficient K^* of the PI/PtBS blend. Furthermore, the orientational coupling (nematic coupling) of PI and PtBS appeared to be rather weak, as explained later in this section. Then, to the first approximation, G^* and K^* can be related to each other through the simplest stress-optical rule[43−46]

$$K^*(\omega) = C_R^{PI} G_{PI}^{bld*}(\omega) + C_R^{PtBS} G_{PtBS}^{bld*}(\omega) \quad (9a)$$

$$G^*(\omega) = G_{PI}^{bld*}(\omega) + G_{PtBS}^{bld*}(\omega) \quad (9b)$$

C_R^{PI} and C_R^{PtBS} are the stress optical coefficients of PI and PtBS in the Rouse/rubbery/flow zones. Note that eq 9b is identical to the formal blending rule explained earlier (which merely represents the stress additivity of the components).

Figure 8a shows the ω dependence of the K^* ($=K' + iK''$) data obtained for the PI128/PtBS348 blend at 100 °C. Both K' and K'' were negative in the entire range of ω examined, and plots of their absolute values, $|K'|$ and $|K''|$, are shown with the circle and square. In the terminal relaxation regime at low ω, the PI chains have fully relaxed to have $G_{PI}^{bld*}(\omega) \ll G_{PtBS}^{bld*}(\omega)$ so that eq 9a is simplified as $K^*(\omega) = C_R^{PtBS} G^*(\omega)$. Thus, we utilized the K'' data at low ω (≤ 0.1 s^{-1}) to evaluate the coefficient for PtBS, $C_R^{PtBS} = K''(\omega)/G''(\omega) = -6.1 \times 10^{-9}$ Pa^{-1} at 100 °C. This C_R^{PtBS} value is close to a value for bulk PtBS, -5.6×10^{-9} Pa^{-1} (100 °C), evaluated from the data at 150 °C ($C_R^{bulk\ PtBS} = -4.9 \times 10^{-9}$ Pa^{-1})[46] after a correction of T; $C_R \propto T^{-1}$. The coefficient for PI, $C_R^{PI} = 1.2 \times 10^{-10}$ Pa^{-1} at 100 °C, was estimated from the bulk PI data,[45] $C_R^{bulk\ PI} = 2.0 \times 10^{-10}$ Pa^{-1} at −40 °C, after the same correction. Utilizing these C_R values at 100 °C in eqs 9a and 9b, we calculated the component moduli G_{PI}^{bld*} and G_{PtBS}^{bld*} from the K^* data and G^* data (obtained in the rheo-optical test at the same frequencies as the K^* data). Figures 8b and 8c show plots of G_{PI}^{bld*} and G_{PtBS}^{bld*}, respectively. The dotted curves in Figure 8c show the G^* data of the blend at low ω. G_{PtBS}^{bld*} coincides with those data (because C_R^{PtBS} was determined from those data).

In parts b and c of Figure 8, the solid curves indicate the component moduli $\phi_X I_X G_X^{bulk*}(\omega\lambda_X)$ (X = PI, PtBS) evaluated on the basis of the blending law, eq 6 combined with eq 4. For PI, $\phi_{PI} I_{PI} G_{PI}^{bulk*}(\omega\lambda_{PI})$ agrees considerably well with the rheo-optically determined $G_{PI}^{bld*}(\omega)$; see Figure 8b. A minor deviation seen between $\phi_{PI} I_{PI} G_{PI}^{bulk*}$ and G_{PI}^{bld*} would be mostly due to the approximate use of G_X^{bulk*} in eq 6, i.e., the approximate replacement of the fast mode distribution in the blend by that in bulk. At high ω (>10 s^{-1}) where eq 6 applies, the deviation between $\phi_X I_X G_X^{bulk*}$ and G_X^{bld*} is larger for PtBS than for PI partly because of this approximation and also of the difference in the magnitudes of G_{PtBS}^{bld*} and G_{PI}^{bld*} (larger than G_{PtBS}^{bld*}): Since the sum $G_{PtBS}^{bld*} + G_{PI}^{bld*}$ is forced to coincide with G^* (eq 9b) and $|G_{PI}^{bld*}|$ is considerably larger than $|G_{PtBS}^{bld*}|$ in the high ω-plateau zone, a minor uncertainty of G_{PI}^{bld*} obtained from the rheo-optical analysis is compensated by a magnified uncertainty of G_{PtBS}^{bld*}. Nevertheless, the deviation between $\phi_{PtBS} I_{PtBS} G_{PtBS}^{bulk*}$ and G_{PtBS}^{bld*} at high ω is still acceptably small, and the results seen in Figures 8, parts b and c, lend support to eq 4 utilized in the blending law approach.

Here, we turn our attention to the orientational coupling[51−57] (nematic coupling) due to the entropic packing interaction[53] (or the excluded volume interaction[54]) of monomeric segments in concentrated systems. This coupling has been experimentally noted for several systems that include binary blends of hydrogenated 1,4-polybutadiene,[51−53] 1,4-polybutadiene (PB) network containing unattached probe PB,[54] and miscible blends of PI and PVE.[55−59] It is well-known that the coupling strongly influences the optical property reflecting the orientation of monomeric segments but negligibly affects the viscoelastic property in long time scales where many monomeric segments are mutually equilibrated to behave as a coarse-grained unit (such as the entanglement segment):[58,59] The orientational coupling constant between the coarse-grained units decreases with increasing unit size thereby resulting in the lack of the coupling effect on the viscoelastic properties in long time scales. Thus, eq 9a is to be modified *if* the PI and PtBS chains in our blends exhibit strong orientational coupling. However, the rheo-optical data suggest rather weak coupling in those blends, as discussed below.

Entangled HPB/HPB blends exhibit strong orientational coupling.[51,52] In those blends, the optical anisotropy of the fast (low-M) component exhibits a slow relaxation tail coupled with the anisotropy of the slow (high-M) component while the stress of the fast component has fully relaxed in this slow tail zone.[51,52] In contrast, the optical anisotropy of PI in the PI/PtBS blend, $C_R^{PI} G_{PI}^{bld*}(\omega)$, *evaluated on the basis of eq* 9a exhibited no slow tail but fully relaxed at $\omega \leq 1/\tau_\varepsilon^{PI}$; see circle and square in Figure 8b. This lack of slow tail cannot be rationalized *if* PI (fast component) were strongly coupled with PtBS (slow component) to violate eq 9a. (The slow tail should be observed *even if eq* 9a *is erroneously applied to a system exhibiting the strong coupling.*) In addition, the stress-optical coefficient C_R^{PtBS} for PtBS evaluated from the data at low ω with the aid of eqs 9a and 9b agreed with

the C_R^{PtBS} data of bulk PtBS, as explained for Figure 8a. This result is consistent with the above argument of weak coupling between PI and PtBS, although it is not a sufficient support for the argument (because $|C_R^{PtBS}|$ is an order of magnitude larger than $|C_R^{PI}|$ so that C_R^{PtBS} evaluated with the aid of eq 9a could still agree with C_R^{PtBS} of bulk PtBS even for the case of strong coupling.)

Thus, the orientational coupling between PI and PtBS appears to be rather weak and eq 9a seems to be valid for our PI/PtBS blends as the first approximation. Of course, the strength of the coupling is dependent on the chemical structure of the components. Details of the coupling between PI and PtBS remain unclear and deserve further investigation.

Finally, a comment needs to be made for the test of the mixing rule conducted in Figures 4−7. This test focused on the viscoelastic moduli in the entanglement plateau zone, and the orientational coupling negligibly affects those moduli.[58,59] Thus, the validity of eq 4 can be unequivocally concluded from the results seen in Figures 4−7, irrespective of the above argument for the coupling.

3-3. Mechanism of Rouse-Like Behavior (Lack of Plateau) at Low *T*. At first sight, the lack of the high-ω entanglement plateau at low T (Figures 1 and 2) might appear to be due to a large contribution of the glassy (segmental) relaxation of PtBS348 to the modulus of the blend. However, this is not the case, as explained below. As shown in Appendix A (Figure 13), bulk PtBS348 exhibits the dielectric and viscoelastic relaxation due to the segmental motion at high ω. On completion of this segmental relaxation, G'' of bulk PtBS348 decreases almost in proportion to ω and becomes considerably larger than G', and G' decreases more strongly down to $\cong 3 \times 10^6$ Pa. (On a further decrease of ω, the segmental contribution to G^* is overwhelmed by the contribution from the Rouse/rubbery mode and the well-known behavior of entangled polymers prevails.) These features should be observed for the G^* data of the PI99/PtBS348 blend at low T (30 °C) *if* the data are dominated by the segmental relaxation of PtBS348. However, as clearly noted in Figure 1, G'' of the blend at 30 °C is not proportional to ω but exhibits the Rouse-like power-law behavior together with G' ($G' = G'' \propto \omega^{1/2}$). Furthermore, a decrease of ω to the low-ω end ($\cong 0.01$ s^{-1}) of this power-law behavior results in a decrease of G' down to $\cong 5 \times 10^4$ Pa, a value much smaller than the minimum value of $0.47 \times 3 \times 10^6 \cong 1.4 \times 10^6$ Pa expected for the modulus sustained by the segmental mode of PtBS348 (having the volume fraction $\phi_{PtBS} = 0.47$ in the blend). Thus, the power-law behavior of the moduli and the corresponding lack of the high-ω entanglement plateau observed for the PI99/PtBS348 blend at 30 °C cannot be attributed to the glassy (segmental) relaxation of PtBS. This conclusion was found for all PI/PtBS blends examined. Furthermore, the glassy relaxation of PtBS is associated with a positive stress optical coefficient[46] but the components of the complex shear optical coefficient, K' and K'', had negative values in the Rouse-like power-law zone, as explained later for Figure 10. This fact also suggests that the glassy relaxation negligibly contributes to the Rouse-like behavior.

Now, it is informative to specify a condition for the entanglement plateau to be observed. The plateau emerges when the Rouse equilibration within the entanglement length a is much faster than the global motion of the chain at a length scale $\gg a$. Consequently, the plateau is not clearly observed if the times required for the Rouse-equilibration and terminal relaxation processes are not widely separated. For high-M homopolymers, these times are well separated because the equilibration rate is determined just by the friction coefficient ζ_s of the Rouse segment without being subjected to a topological constraint. In contrast, in the PI/PtBS blends at low T, ζ_s is much larger for PtBS than for PI and thus the *intrinsic* Rouse equilibration time over the length a, $\tau_a^\circ = \zeta_s a^2 N_R/6\pi^2 k_B T \propto \zeta_s$ with N_R being the number of the Rouse segments *per* entanglement segment ($a = b_R N_R^{1/2}$ with b_R = Rouse segment size), is much longer for PtBS. Obviously, the PI chain cannot take a conformation penetrating a space occupied by the PtBS segments. Thus, the slow PtBS chains should *topologically* hinder the PI chain from exploring, within the intrinsic $\tau_{a,PI}^\circ$, all *local* conformations at a length scale of a. For this case, the PI and PtBS chains should be cooperatively equilibrated at a rate determined by the PtBS motion. Specifically, for the cooperative equilibration over a length scale $\xi(t)$ larger than the Rouse segment size b_R ($\sim$1 nm), $\xi(t)$ would increase with t as $\xi(t) \sim a(t/\tau_{a,PtBS}^\circ)^{1/4}$. Note that the growth rate of $\xi(t)$ is determined by the intrinsic $\tau_{a,PtBS}^\circ$ of PtBS. During this equilibration process, the PI segment should fluctuate (in a cage of size ξ) *much faster* than the PtBS segment. Namely, during one cycle of fluctuation of the PtBS chain conformation within the length ξ, the PI chain conformation should rapidly fluctuate many times within the same ξ at a frequency determined by $\zeta_{s,PI}$ ($\ll \zeta_{s,PtBS}$).

The above argument suggests that the PI chain fully relaxes soon after its cooperative Rouse equilibration over the length a thereby exhibiting no clear entanglement plateau at high ω *if* $\tau_{a,PtBS}^\circ$ is not very shorter than the terminal entanglement relaxation time of PI. This could be the mechanism of the lack of the high-ω entanglement plateau noted for the PI/PtBS blends at low T. (One may argue that the PI and PtBS chains are equilibrated separately and the lack of the high-ω plateau results from the orientational coupling of the PI and PtBS chains. However, the cooperative equilibration appears to be quite reasonable in the length scale $\xi > b_R$ and this mechanism of the lack of plateau seems to be unlikely, as discussed later in more detail.)

We can test the molecular picture of cooperative Rouse equilibration for the data shown in Figure 1. For a chain of the molecular weight M and mass concentration C, the Rouse power-law behavior of G' and G'' can be compactly expressed in a continuous form,[60]

$$G'(\omega) = G''(\omega) = 1.111\frac{CRT}{M}(\omega\tau_{G,R})^{1/2} \qquad (10)$$

where R is the gas constant and $\tau_{G,R}$ is the viscoelastic Rouse relaxation time. For the PI99/PtBS348 blend (w_{PI} = 50 wt %) at 30 °C, we can replace M in eq 10 by the entanglement molecular weight of the component X therein (X = PI, PtBS), $M_e^X = \{a/a_X^{bulk}\}^2 M_e^{bulk\ X}$ with a = 6.3 nm (cf. eq 4), to estimate the modulus corresponding to the Rouse equilibration over the length a:

$$G'(1/\tau_a) = G''(1/\tau_a) = 1.111\left\{\frac{C_{PI}RT}{M_e^{PI}} + \frac{C_{PtBS}RT}{M_e^{PtBS}}\right\}$$
$$= 3.6 \times 10^5 \text{ Pa} \qquad (11)$$

Here, τ_a is the Rouse equilibration time that is common for PI and PtBS in the blend (as discussed above), and $1/\tau_a$ ($=\omega_a$) is the corresponding frequency. From the modulus data for the PI99/PtBS348 blend at 30 °C (Figure 1), we find that $G' = G'' = 3.6 \times 10^5$ Pa at $\omega_a = 0.4$ s^{-1}. The corresponding Rouse equilibration

time, τ_a = 2.5 s, is just moderately shorter than the dielectrically observed terminal relaxation time of PI, τ_ε^{PI} = 10 s. (This τ_a is indeed close to the intrinsic $\tau_{a,PtBS}^{\circ}$ of PtBS in the blend, as explained below.) Thus, the PI chain exhibits the terminal relaxation soon after its retarded Rouse equilibration. This result, found for all PI/PtBS blends at low T, lends support to the above molecular picture attributing the lack of the high-ω plateau to the retardation of the Rouse equilibration of the PI chains.

The intrinsic Rouse relaxation time of bulk PtBS is available in linearature:[41] $\tau_{a,bulk}$ = 1.6 s for $M_{PtBS} = M_e^{bulkPtBS} = 37.6 \times 10^3$ at T = 180 °C (this $\tau_{a,bulk}$ value can be confirmed also for the G^* data of bulk PtBS348 shown in Appendix A). Previous WLF analysis[38] gave the *iso*-τ_s temperatures (often referred to as *iso*-frictional temperatures), T_{iso}, where the Rouse segment in blends and bulk has the same local relaxation time τ_s ($\sim\zeta_s b_R^2/k_BT$). Specifically, $T_{iso\text{-}PtBS}$ = 43 °C and $T_{iso-PtBS}^{bulk}$ = 180 °C for PtBS in the 50 wt % PI/PtBS blend and in bulk, respectively.[38] Thus, the intrinsic $\tau_{a,PtBS}^{\circ}$ of PtBS over the entanglement length a in the 50 wt % blend is evaluated to be $\tau_{a,PtBS}^{\circ} = r_M 10^{\Delta}\tau_{a,bulk}(180\ ^\circ C) = 2.4$ s at 30 °C. Here, $r_M = \{M_e^{PtBS}/M_e^{bulkPtBS}\}^2 = \{a/a_{PtBS}^{bulk}\}^4 = 0.084$, and Δ is the logarithmic WLF shift factor for PtBS in the blend from $T_{iso\text{-}PtBS}$ = 43 °C to T = 30 °C: $\Delta = -10(T - T_{iso\text{-}PtBS})/(116.5 + T - T_{iso\text{-}PtBS}) = 1.26$ (cf. eq A2 shown in Appendix A). This $\tau_{a,PtBS}^{\circ}$ excellently agrees with τ_a (= 2.5 s) evaluated above, suggesting that the Rouse equilibration of the PtBS99 chains in the blends occurs through their intrinsic Rouse mode.

The intrinsic Rouse equilibration time of PI in the 50 wt % blend, $\tau_{a,PI}^{\circ} = 1.1 \times 10^{-4}$ s at 30 °C, was similarly evaluated from the WLF shift factor[38] (cf. eq A1 in Appendix A) and the data for bulk PI ($\tau_{a,bulk} = 3.4 \times 10^{-6}$ s for $M_{PI} = M_e^{bulkPI} = 5.0 \times 10^3$ at T = 30 °C).[30−33] This $\tau_{a,PI}^{\circ}$ is orders of magnitude shorter than $\tau_{a,PtBS}^{\circ}$ (=2.4 s at 30 °C), confirming that the equilibration of PI in the blend over the length a is topologically hindered/retarded by the PtBS chains.

In relation to the above molecular picture of cooperative equilibration, we also note that the G' data at *high* T shown in Figures 1 and 4−7 have values smaller than the $G'(1/\tau_a)$ value specified by eq 11; $10^{-5}G'(1/\tau_a)$/Pa = 4.5, 4.4, and 4.2 for (w_{PI}/wt %, T/°C) = (56, 80), (50, 100), (40, 120), respectively. In addition, the intrinsic $\tau_{a,PtBS}^{\circ}$ of PtBS evaluated with the method explained above, $\tau_{a,PtBS}^{\circ} = 6.8 \times 10^{-5}$ s for the 50 wt % blend at 100 °C, is much smaller than the shortest time scale (1×10^{-3} s) examined in Figure 1. These results indicate that at high T the PtBS chains had been already equilibrated over the length a in our experimental window. Thus, the PI chain should have been also equilibrated cooperatively to have $\tau_\varepsilon^{PI} \gg \tau_a$ ($=\tau_{a,PtBS}^{\circ}$), as noted in Figure 1. This large difference between τ_ε^{PI} and τ_a enabled the PI chains to exhibit the high-ω plateau of G' (at $\omega < 1/\tau_a$) together with the PtBS chains, as noted in Figures 4−7. Thus, the emergence of the high-ω plateau at high T is in harmony with the above molecular picture. (One may argue that the PI and PtBS chains are equilibrated separately. However, the cooperative equilibration seems to be quite reasonable in a length scale > Rouse segment size ~1 nm, as discussed later in more detail.)

3.4. Model for Blend Modulus at Low *T*. From the molecular picture of the cooperative Rouse equilibration of the PI and PtBS chains over the entanglement length a, the complex modulus of the PI chains in the PI/PtBS blends at low T can be modeled as

$$G_{PI}^{bld}*(\omega) = \frac{C_{PI}RT}{M_e^{PI}}\sum_{p=1}^{N_R}\frac{i\omega\tau_a/r_p^2}{1 + i\omega\tau_a/r_p^2} + \phi_{PI}I_{PI}G_{PI}^{bulk}*(\omega\lambda_{PI}') \quad (12a)$$

with

$$r_p = \sin\left\{\frac{p\pi}{2(N_R + 1)}\right\}\sin^{-1}\left\{\frac{\pi}{2(N_R + 1)}\right\} \quad (12b)$$

In eq 12a, $M_e^{PI} = \{a/a_{PI}^{bulk}\}^2 M_e^{bulk\ PI}$ is the entanglement molecular weight for PI in the blend, and N_R is the number of Rouse segments (more accurately, the number of the Rouse bond vectors) per entanglement segment of the size a. Since the Rouse and Kuhn segments of flexible PI chains are similar in size, we may estimate this number as $N_R = M_e^{PI}/M_{Kuhn}^{PI}$. The first summation term including these parameters represents the discrete Rouse process with the equilibration time τ_a (determined by PtBS). The second term represents the terminal entanglement relaxation of PI occurring at the dielectric relaxation time in the blend, τ_ε^{PI}. (Since the global motion is much faster for PI than for PtBS, the terminal viscoelastic relaxation time of PI can be safely replaced by the dielectric τ_ε^{PI}, as explained earlier.) As explained for eq 6, we approximately expressed this term in terms of the bulk PI modulus $G_{PI}^{bulk}*$, the PI volume fraction ϕ_{PI}, the relaxation time shift factor $\lambda_{PI}' = \tau_\varepsilon^{PI}/\tau_G^{bulk\ PI}$, and the factor I_{PI} (given by eq 8a) representing a change of the entanglement plateau on blending.

Now, we turn our attention to the PtBS chains in the blend. These chains are also Rouse-equilibrated over the entanglement length a with the characteristic time τ_a. Since the PtBS and PI chains are equilibrated cooperatively to have the common τ_a, the onset time of the Rouse equilibration, $\tau_a/r_{N_R}^2$ (cf. eq 12b), would be also common for these chains. Thus, we may approximately replace the number of the Rouse segment per entanglement segment of PtBS in the blend by N_R of the PI chain. After this equilibration (over a length scale of $\xi(t) \sim a(t/\tau_a)^{1/4}$ at time $t \le \tau_a$), the global motion of PI chains would activate the CR relaxation of the PtBS chain thereby dilating the entanglement mesh size for PtBS from a (described by eq 4) to the size in the PtBS solution having the same volume fraction ϕ_{PtBS} as the blend, $a_{soln} = a_{PtBS}^{bulk}/\phi_{PtBS}^{0.65}$. After this CR/dilation process, the effective entanglement molecular weight for PtBS agrees with that in the solution, $M_e^{soln} = M_e^{bulk\ PtBS}/\phi_{PtBS}^{1.3}$, and PtBS exhibits the terminal relaxation in the dilated entanglement mesh characterized by this M_e^{soln}. Thus, in a range of ω where this terminal relaxation has *not* occurred, the PtBS modulus can be modeled as

$$G_{PtBS}^{bld}*(\omega) = \frac{C_{PtBS}RT}{M_e^{PtBS}}\sum_{p=1}^{N_R}\frac{i\omega\tau_a/r_p^2}{1 + i\omega\tau_a/r_p^2} + \frac{C_{PtBS}RT}{M_e^{soln}}\sum_{p=1}^{N_{CR}-1}\frac{i\omega\tau_{CR}/q_p^2}{1 + i\omega\tau_{CR}/q_p^2} + \frac{C_{PtBS}RT}{M_e^{soln}} \quad (13a)$$

with

$$q_p = \sin\left\{\frac{p\pi}{2N_{CR}}\right\}\sin^{-1}\left\{\frac{\pi}{2N_{CR}}\right\} \quad (13b)$$

Here, $M_e^{PtBS} = \{a/a_{PtBS}^{bulk}\}^2 M_e^{bulk\ PtBS}$ is the PtBS entanglement molecular weight in the blend (in the high-ω plateau zone), and r_p is given by eq 12b. In eq 13a, the first term represents the Rouse equilibration of the PtBS chain, the second term indicates the Rouse-type CR process[2,3,61] having the longest characteristic time τ_{CR}, and the third term denotes the dilated entanglement plateau identical to that in the solution. The number of the CR segments N_{CR}, specifying the upper bound of the second summation in eq 13a and determining the q_p factor in eq 13b, is taken

Table 2. Parameter Values Utilized in the Model

	PI99/PtBS348, w_{PI} = 50 wt %, 30 °C	PI128/PtBS348, w_{PI} = 50 wt %, 30 °C	PI128/PtBS348, w_{PI} = 40 wt %, 60 °C
a/nm[a]	6.3	6.3	6.5
τ_a/s[b]	2.5	2.5	1.0
τ_ε^{PI}/s[c]	10	20	2.8
$10^{-3}M_e^{PI}$[d]	5.8	5.8	6.2
$10^{-3}M_e^{PtBS}$[d]	10.8	10.8	11.5
N_R[e]	44	44	47
N_{CR}[f]	9	9	7
$10^{-2}\tau_{CR}$/s[g]	2.7	5.5	0.47

[a] Determined from eq 4. [b] Evaluated from G* data (cf. eq 11). [c] Evaluated from ε'' data. [d] $M_e^X = \{a/a_X^{bulk}\}^2 M_e^{bulk\ X}$ (X = PI, PtBS). [e] $N_R = M_e^{PI}/M_{Kuhn}^{PI}$ [f] $N_{CR} = M_e^{soln}/M_e^{PtBS}$. [g] $\tau_{CR} = \Lambda(z)\tau_\varepsilon^{PI} q_{N_{CR}-1}^{-2}$ (cf. eqs 13b and 14).

to be the number of the entanglement segments of PtBS *per* dilated entangled mesh and evaluated as $N_{CR} = M_e^{soln}/M_e^{PtBS}$. Since the local CR hopping of the PtBS chain is activated by the global motion of the PI chains, the onset time for the CR process, $\tau_{CR}/q_{N_{CR}-1}^2$, should be proportional to τ_ε^{PI} of PI. Utilizing the Graessley model,[61] we may relate $\tau_{CR}/q_{N_{CR}-1}^2$ and τ_ε^{PI} as

$$\tau_{CR}/q_{N_{CR}-1}^2 = \Lambda(z)\tau_\varepsilon^{PI}, \quad \text{with } \Lambda(z) = \frac{1}{z}\left(\frac{\pi^2}{12}\right)^z \qquad (14)$$

Here, z is the local jump gate number typically in a range of z = 2−4. We treat z as an adjustable parameter to evaluate τ_{CR} from the τ_ε^{PI} data and a chosen value of z (= 2 for all blends, as shown later).

The basic times appearing in eqs 12a and 13a, τ_a and τ_ε^{PI}, have been determined from the viscoelastic and dielectric data as explained in the previous section. The other parameters, M_e^X (X = PI, PtBS), N_R, N_{CR}, and τ_{CR} were evaluated from a (eq 4), a_X^{bulk} and $M_e^{bulk\ X}$ (eqs 1 and 2), M_{Kuhn}^{PI}(= 130), M_e^{soln} (= $M_e^{bulk\ PtBS}/\phi_{PtBS}^{1.3}$), and τ_ε^{PI}. The values of these parameters are summarized in Table 2. Utilizing those values, we can compare the blend modulus calculated from the model (eqs 12a and 13a) with the $G^*(\omega)$ data at low T. The results of this comparison are shown in Figure 9. Since the model approximates the modulus of PI in the blend by the bulk modulus (cf. eq 12a), no perfect agreement is expected between the model and experiments. Nevertheless, Figure 9 demonstrates that the modulus calculated from the model with a reasonable value of z = 2 (solid curves) is surprisingly close to the data for all blends examined (symbols).[62] (The orientational coupling, *even if* prevailing in the PI/PtBS blends, negligibly affects the modulus in long time scales and thus has no influence for the result seen in Figure 9.) The close coincidence of the model calculation and the data lends support to the molecular picture underlying the model, the cooperative Rouse equilibration of the PI and PtBS chains that is slower than the intrinsic Rouse equilibration of PI and leads to the lack of high-ω plateau at low T.

We may utilize the preliminary rheo-optical data to further test the model. Figure 10a shows the complex shear optical coefficient K^* ($=K' + iK''$) measured for the PI128/PtBS348 blend with w_{PI} = 50 wt % at 30 °C. K' was negative in the entire range of ω examined, and K'' was also negative at $\omega < 100\ s^{-1}$ where the blend exhibited the Rouse-like power-law behavior. Thus, the plots are shown for their absolute values, $|K'|$ and $|K''|$. The negative sign of K' and K'' suggests that the segmental relaxation of PtBS hardly contributes to the blend moduli in our experimental window, as

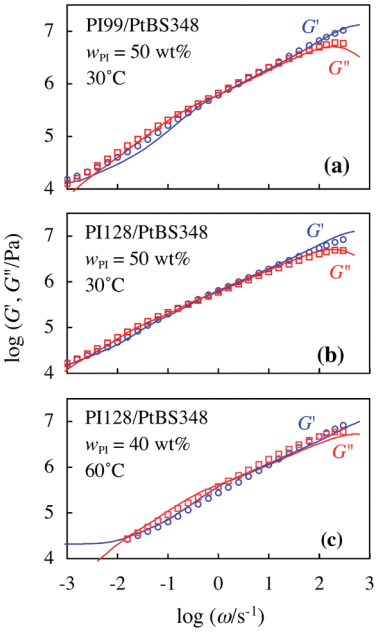

Figure 9. Comparison of the model prediction (eqs 12a and 13a; solid curves) with the G^* data at 30 °C measured for the PI/PtBS blends as indicated.

explained earlier. Furthermore, the orientational coupling between the PI and PS chains appear to be rather weak, as discussed earlier. Thus, as the first approximation, the K^* and G^* data can be analyzed within the framework of the stress-optical rule, eq 9, to give the component moduli.

Applying the temperature correction ($C_R \propto T^{-1}$) to the stress optical coefficients C_R at 100 °C (utilized for Figure 8), we evaluated C_R at 30 °C: $C_R^{PtBS} = -5.0 \times 10^{-9}$ Pa^{-1} and $C_R^{PI} = 9.7 \times 10^{-10}$ Pa^{-1}. $G_{PI}^{bld*}(\omega)$ and $G_{PtBS}^{bld*}(\omega)$ evaluated from eq 9 with these C_R values are shown with the symbols in Figures 10b and 10c, respectively. These rheo-optically obtained moduli are very close to the moduli deduced from the model (eqs 12a and 13a; shown with the curves), in particular at middle to low ω where the retarded Rouse equilibration is followed by the entanglement relaxation and the CR/entanglement mesh dilation.[63] This result demonstrates the basic validity of the model.

3.5. Dielectric Mode Distribution of PI in Blend. Here, we turn our attention to the dielectric mode distribution of the PI chains in the blends. On a decrease of T, the slow dynamics of PI changes from the reptation-like dynamics in the entanglement

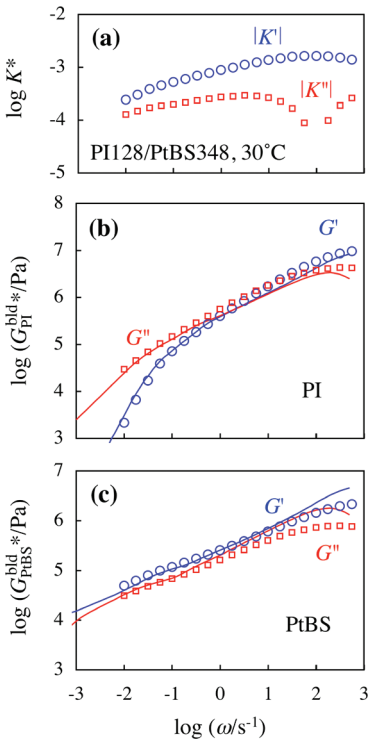

Figure 10. (a) Complex shear optical coefficient of PI128/PtBS348 blend (w_{PI} = 50 wt %) at 30 °C. (b and c): Comparison of the rheo-optically determined component moduli (symbols) with the moduli deduced from the model, eqs 12 and 13 (curves).

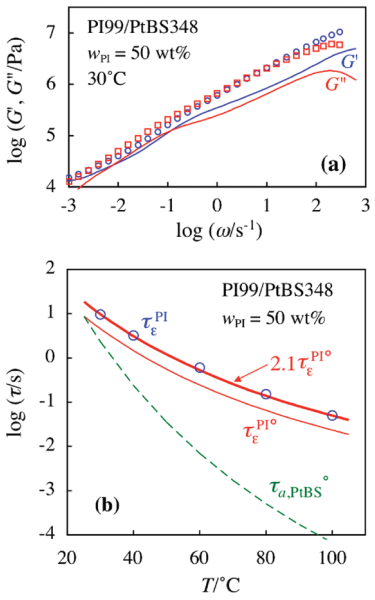

Figure 11. (a) Test of possibility of separate Rouse equilibration of PI and PtBS chains in the blend. The G^* data of the blend (symbols) are compared with the prediction of the model assuming the separate equilibration. (b) Test of possibility of the reptation-like terminal relaxation of PI chain immediately after the cooperative Rouse equilibration. The terminal relaxation time τ_ε^{PI} of the PI99 chain in the blend (circle) is compared with the time $\tau_\varepsilon^{PI^\circ}$ expected for the reptation relaxation equivalent to that in bulk PI system (solid curves) and with the intrinsic Rouse equilibration time $\tau_{a,PtBS}{}^\circ$ of PtBS in the blend (dashed curve). For details, see text.

mesh equilibrated through the fast Rouse process to the retarded Rouse equilibration dynamics under the topological hindrance from the slow PtBS chains (immediately followed by the terminal reptative dynamics), as discussed earlier. Nevertheless, the dielectric mode distribution of PI is insensitive to this change thereby allowing the ε'' data to obey the time−temperature superposition (Figure 2). This result can be related to a fact that the dielectric mode distribution of PI, equivalent to the distribution of the end-to-end vector fluctuation modes, is very similar for the reptation-like and Rouse-like dynamics.[2,34] Thus, the change of the slow dynamics of PI still allowed the ε'' data to obey the superposition.

In Figure 2, the solid curve shows the ε'' data of bulk PI99 at T_r = 30 °C corrected for the PI volume fraction in the blend (ϕ_{PI} = 0.53) and shifted along the ω axis to match the ε'' peak frequency with that for the data in the blend. The dielectric mode distribution of PI in the blend is close to but a little broader than that of bulk PI. This delicate difference may be related to motional constraint from PtBS and the frictional heterogeneity, both resulting from the composition fluctuation essentially quenched in the time scale of PI relaxation.[36,38] Further details of the dielectric mode distribution in the blends will be examined in our future work.

3.6. Possibility of Other Relaxation Mechanism(s) in Blend. The molecular picture of cooperative Rouse equilibration of the PI and PtBS chains over the length a (with the rate determined by PtBS) is consistent with the experimental observation at low and high T, as discussed in the previous sections. This molecular picture, incorporated also in the experimentally confirmed mixing rule (eq 4), is very reasonable. However, one may argue that the PI chains are possibly equilibrated more quickly than the PtBS chains and the orientational coupling of the PI segments with the slow PtBS segments possibly results in the lack of the high-ω entanglement plateau at low T. These possibilities are examined below.

The possibility of separate equilibration of the PI and PtBS chains (faster for the former) can be most straightforwardly examined for the G^* data of the blends at low T with the aid of the model (eqs 12a and 13a). The equilibration time τ_a utilized in the model was in excellent agreement with the intrinsic $\tau_{a,PtBS}{}^\circ$ (= 2.4 s) obtained for PtBS in the 50 wt % PI99/PtBS blend at 30 °C, as explained earlier. If the PI99 chain therein were equilibrated separately through its intrinsic Rouse mode, the high-ω data of the blend dominated by the (separate) equilibration process should be described by the model with τ_a in eq 12a being replaced by $\tau_{a,PI}{}^\circ$ (=1.1 × 10^{-4} s, as evaluated earlier). In fact, the model prediction at $\omega > 1\ s^{-1}$ did not change significantly even if the terms in eqs 12a and 13a other than the first terms were eliminated, meaning that the moduli at $\omega > 1\ s^{-1}$ were dominated by the equilibration process. In Figure 11a, the G^* data of the blend at 30 °C (symbols) are compared with this modulus calculated with $\tau_a = \tau_{a,PI}{}^\circ$ for PI (curves). The calculation significantly underestimates G^* at high $\omega > 1\ s^{-1}$ (equilibration dominant zone), indicating that the actual equilibration of the PI99 chain in the blend is much slower than its intrinsic Rouse equilibration and should occur cooperatively with the PtBS348 chain. (This underestimation cannot be related to the orientational coupling because the coupling negligibly affects the G^* data.[58,59])

We also note a conceptual difficulty for the separate equilibration of the PI and PtBS chains over a length ξ larger than the

Rouse segment size b_R (~1 nm) because the PI chain cannot take a local conformation penetrating a space occupied by the PtBS segments so that motion of the PtBS segments is required for the PI chain to explore all local conformations. This point can be further examined quantitatively for the 50 wt % PI99/PtBS blend at 30 °C for which the characteristic time for the intrinsic Rouse equilibration over the length a (= 6.3 nm) is known: $\tau_{a,PI}^{\circ} = 1.1 \times 10^{-4}$ s for PI and $\tau_{a,PtBS}^{\circ} = 2.4$ s for PtBS. The length scale for the fluctuation of the PtBS segment in a time scale of $\tau_{a,PI}^{\circ}$ is estimated to be $\xi_{PtBS} \sim a(\tau_{a,PI}^{\circ}/\tau_{a,PtBS}^{\circ})^{1/4} \cong 0.5$ nm $< b_R$. Namely, in the time scale of $\tau_{a,PI}^{\circ}$, the Rouse segments of PtBS hardly move and behave as immobilized objects densely distributed in space (at the volume fraction of $\phi_{PtBS} = 0.47$). In this situation, it is quite unlikely that the PI chain can explore all local conformations in the length scale a within its intrinsic $\tau_{a,PI}^{\circ}$.

Of course, the real chains exhibit very local motion of the monomeric segments at a length scale $< b_R$ (~1 nm) and such local motion can occur at different rates for different components.[6−22] Quasielastic neutron scattering experiments[64] suggested that the correlation of this local motion vanishes at $\xi \cong 0.8$ nm. Thus, for the chemically different components in the entangled blends, there should be a crossover from the almost independent, local motion (for $\xi \leq b_R$) to the highly cooperative motion/equilibration (for $b_R < \xi \leq a$) and further to the global motion (for $a < \xi$) that corresponds to the entanglement relaxation (during which different chains are motionally correlated to some extent through the CR and other mechanisms). This crossover is beyond the scope of this study and is considered to be a very important subject of future work.

Now, we examine if the lack of the high-ω entanglement plateau in the PI/PtBS blends at low T results from the orientational coupling (nematic coupling) of the PI and PtBS chains. This coupling appears to be rather weak but could still have affected the rheo-optical data to some extent, as discussed for Figure 8. Nevertheless, the coupling itself negligibly affects the viscoelastic moduli in long time scales where many monomeric segments are mutually equilibrated to behave as a larger coarse-grained unit.[58,59] The orientational coupling constant between the coarse-grained units decreases with increasing unit size because of the mutual equilibration of the monomeric segments in each unit, which leads to the lack of the coupling effect on the moduli in long time scales including the Rouse relaxation zone.[58,59] Thus, the lack of the high-ω entanglement plateau of the PI/PtBS blends at low T is not attributed to the orientational coupling but to the mechanism of the cooperative Rouse equilibration.

Finally, one may also argue that the global relaxation of PI results from accumulation of the local equilibration (over the length a) and thus the reptation-like relaxation of PI cannot occur given that the equilibration time τ_a is not much shorter than the dielectrically detected terminal relaxation time of PI, τ_ε^{PI}. However, once the cooperative Rouse equilibration of the PI and PtBS chains is completed at $t = \tau_a$, the PI chain becomes free from the local topological hindrance from the PtBS chain at the length scale $< a$ and the time for reptation of the PI chain at a larger scale ($>a$) would be essentially determined by the contour length of the PI chain, $a\{M_{PI}/M_e^{PI}\}$, as well as the total friction of the PI chain, $\zeta_{PI\text{-chain}} = \zeta_{s,PI}N_R\{M_{PI}/M_e^{PI}\}$ where $\zeta_{s,PI}$ is the friction coefficient of the Rouse segment of PI in the blend and N_R is the number of those segments per entanglement segment. This reptation time can be close to τ_a ($=\tau_{a,PtBS}^{\circ}$) determined by the PtBS motion. In other words, the PI chain can fully relax through its reptation-like motion in the entanglement mesh of the size a immediately after the cooperative Rouse equilibration. This point is further examined below.

We made the WLF shift for the $\tau_\varepsilon^{bulk\ PI}$ data for bulk PI99 to reduce those data to the iso-τ_s state defined with respect to the PI99 chain in the 50 wt % PI99/PtBS348 blends at various T examined in Figure 2. We further corrected those shifted data for a small change of M_e on blending to evaluate the dielectric relaxation time expected for the PI99 chain in the blend relaxing through the *same* mechanism as in its bulk state, $\tau_\varepsilon^{PIo} = \{M_e^{PI}/M_e^{bulk\ PI}\}^{-1.5}\tau_\varepsilon^{bulk\ PI}$. Here, the minor correction factor $\{M_e^{PI}/M_e^{bulk\ PI}\}^{-1.5}$ (= 0.8) accounts for the relationship between τ_ε^{PI} and M_e, $\tau_\varepsilon^{PI} \propto M_e^{-1.5}$. In Figure 11b, the τ_ε^{PIo} thus evaluated (thin solid curve) is compared with τ_ε^{PIo} data for the PI99 chain in the 50 wt % PI99/PtBS348 blend at various T (circles). The thick solid curve shows τ_ε^{PIo} multiplied by a factor of 2.1. The intrinsic $\tau_{a,PtBS}^{\circ}$ of PtBS in the blend, evaluated from the WLF shift and the M_e^{PtBS}-correction for the bulk PtBS data explained earlier, is also shown; cf. dashed curve. Clearly, the τ_ε^{PIo} data are very close, in both magnitude and T dependence, to $2.1\tau_\varepsilon^{PIo}$. This result strongly suggests that the PI99 chain exhibits the reptation-like terminal relaxation similar to that in its bulk system even at low T (30 °C) where the cooperative Rouse equilibration time τ_a ($=\tau_{a,PtBS}^{\circ}$) is shorter than τ_ε^{PI} only by a factor of 4. The moderate difference between τ_ε^{PI} and τ_ε^{PIo} (by a factor of 2.1) would reflect the long lifetime of the entanglement constraint from PtBS348 (slow component) to PI99 (fast component). A similar, moderate difference was noted in a previous study for moderately entangled PI/PtBS blends.[38]

3.7. Additional Comments. In all high-M blends examined in this study, the terminal relaxation of PI was dielectrically observed at ω where the modulus was below $G^*(1/\tau_a)$ for the Rouse equilibration over the entanglement length a (cf. eq 11), although the terminal relaxation time τ_ε^{PI} was not significantly longer than the equilibration time τ_a at low T. This situation was confirmed also for most of low-M, lightly entangled PI/PtBS blends examined in the previous studies.[36,38] For those low-M blends as well as the high-M blends examined in this study, we can utilize the $G_{PI}^{bulk*}(\omega)$ data of bulk PI to approximate the modulus of PI in the blend at $\omega < 1/\tau_a$ as $G_{PI}^{bld*}(\omega) = \phi_{PI}I_{PI}G_{PI}^{bulk*}(\omega\lambda_{PI})$ (cf. eq 6). Thus, *if* we intend to experimentally examine the relaxation behavior of PtBS, we can safely subtract this $G_{PI}^{bld*}(\omega)$ from the $G^*(\omega)$ data of the blend to evaluate $G_{PtBS}^{bld*}(\omega)$ of PtBS at $\omega < 1/\tau_a$ (in addition to the direct, rheo-optical determination of G_{PtBS}^{bld*}). Indeed, this subtraction was successfully made in the previous studies[36,38] to examine the thermorheological behavior of PtBS in the low-M blend.[65]

In relation to the above argument, we expect an interesting situation that the PI chains behave as the fast component and are entangled with the PtBS chains but fully relax before the Rouse-equilibration over the entanglement length a is completed. For this case, a submolecule of the size $< a$, instead of the entanglement segment, may behave as the motional unit during the terminal relaxation of PI. This situation would be realized in PI/PtBS blends with adequately chosen values of M_{PI}, M_{PtBS}, and ϕ_{PtBS} and at adequate T. The component dynamics in those blends is considered to be a very interesting subject of future work.

4. CONCLUDING REMARKS

We have examined the viscoelastic, dielectric, and rheo-optical behavior of well-entangled PI/PtBS blends in the miscible state.

The component dynamics therein, in particular that of PI (fast component), changed with T significantly.

At high T, the blend exhibited two-step entanglement plateau of the storage modulus G'. The high-ω and low-ω plateaus were attributed to the entanglement among all component chains and that between the PtBS chains (slow component), respectively. The entanglement length a characterizing the high-ω plateau was well described by the simple mixing rule based on the number fraction n of the Kuhn segments of the components, $a=n_{PI}a_{PI}^{bulk} + n_{PtBS}a_{PtBS}^{bulk}$. This result is consistent with the current molecular picture that relates the entanglement density to the packing length p ($\cong a/20$). Furthermore, in the high-ω plateau zone, the component moduli obtained from a blending law combined with this mixing rule of a were close to the rheo-optically determined moduli. This result lent further support to the above mixing rule of a.

At low T, the blend exhibited the Rouse-like power-law behavior of moduli ($G' = G'' \propto \omega^{1/2}$) at ω where the high-ω plateau was supposed to emerge. This lack of the high-ω plateau was attributed to retardation of the Rouse equilibration of the PI chain over the entanglement length a due to the topological hindrance from the slow PtBS chains. In other words, the PI and PtBS chains were equilibrated cooperatively at a rate determined by PtBS. This equilibration time τ_a, evaluated from the G^* data of the blend, agreed with the intrinsic Rouse equilibration time of PtBS in the blend. τ_a was shorter than the dielectrically detected terminal relaxation time of PI τ_ε^{PI}, but the difference between τ_a and τ_ε^{PI} was small. Thus, the high-ω plateau zone was too narrow to be resolved experimentally, and the PI chains relaxed almost immediately after their Rouse equilibration cooperative with PtBS. This PI relaxation activated the CR relaxation of PtBS to dilate the entanglement mesh size for PtBS to that in the corresponding PtBS solution. A simple model considering the Rouse equilibration and CR/dilation processes described the G^* data of the blend surprisingly well, lending support to the molecular picture underlying the model, the cooperative/simultaneous Rouse equilibration of PI and PtBS chains. The model prediction was consistent with the rheo-optical data, which lent further support to this picture.

Finally, it should be emphasized that the cooperative Rouse equilibration is intimately related to the fundamental aspect of polymer rheology that the mechanical stress reflects the orientational anisotropy of submolecules exploring all internal conformations in a given time scale. At low T, the PI chain *cannot* explore all conformations at length scales $\leq a$ within its intrinsic Rouse time $\tau_R^{PI}(a)$ because the slow PtBS chains behave as densely dispersed obstacles in this time scale thereby hindering the PI chain from this exploration. The chain motion is accelerated with increasing T more significantly for PtBS than for PI, which enables this exploration to occur quickly (at $t \ll \tau_\varepsilon^{PI}$). The PI/PtBS blends exhibit the high-ω plateau only at such high T.

APPENDIX A

Dynamic Behavior of Bulk PI and PtBS. Viscoelastic and dielectric behavior was examined for the PI and PtBS components in respective bulk states. Figure 12 shows the master curves of G^* and ε'' measured for bulk PI99 and PI128, and Figure 13, for bulk PtBS348.[41] The shift factors a_T in the Rouse/rubbery/flow zone were well described by the previously reported WLF equations,[38]

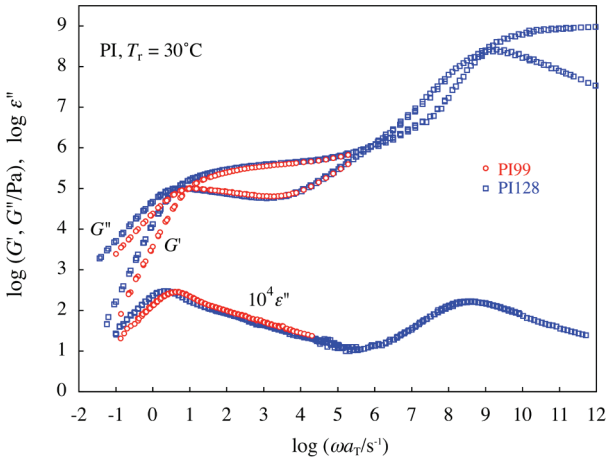

Figure 12. Viscoelastic and dielectric data of bulk PI99 and PI128 at 30 °C.

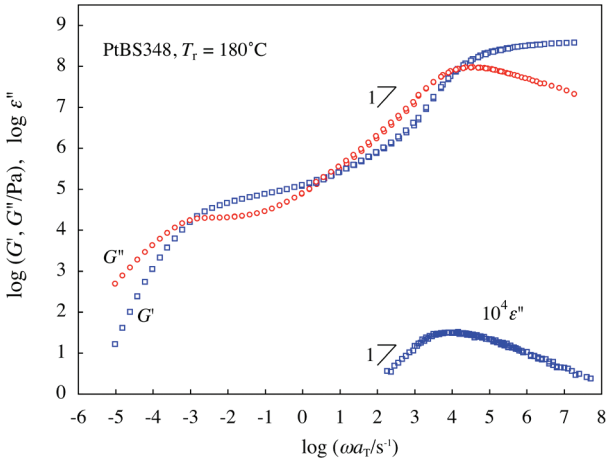

Figure 13. Viscoelastic and dielectric data of bulk PtBS348 at 180 °C.

$$\log a_T = -\frac{4.425(T - T_r)}{140.0 + T - T_r} \quad \text{with} \quad T_r = 30\ ^\circ\text{C for PI99 and PI128} \tag{A1}$$

$$\log a_T = -\frac{10.0(T - T_r)}{116.5 + T - T_r} \quad \text{with} \quad T_r = 180\ ^\circ\text{C for PtBS348} \tag{A2}$$

PI has the type-A dipole parallel along the chain backbone and its global motion activates both viscoelastic and dielectric relaxation, while PtBS has no type-A dipole and its global motion is dielectrically inert; see Figures 12 and 13. This feature, enabling us to attribute the *slow* dielectric relaxation of the PI/PtBS blends exclusively to the global motion of PI therein, was very useful for the analysis of the component dynamics, as demonstrated in Figures 4−7, 9, and 10.

Both PI and PtBS have type-B dipoles perpendicular to the chain backbone and thus their segmental (glassy) viscoelastic relaxation seen at high ω is associated with the dielectric relaxation. The dielectric intensity of the segmental relaxation of PtBS,

$\Delta\varepsilon_{seg}^{PtBS}$, is considerably smaller than $\Delta\varepsilon_{seg}^{PI}$ of PI and even smaller compared to the intensity $\Delta\varepsilon_{global}^{PI}$ of the global relaxation of PI ($\Delta\varepsilon_{seg}^{PtBS} \cong 0.27\Delta\varepsilon_{seg}^{PI} \cong 0.21\Delta\varepsilon_{global}^{PI}$ at the same T). Thus, the segmental relaxation of PtBS could hardly contribute to the dielectric data of the blends at frequencies of the global PI relaxation *even if* the segmental relaxation *was supposed to* occur at those frequencies. Actually, the segmental relaxation of both PI and PtBS was completed in our experimental window for the blends so that its contribution to the data is negligibly small.

Finally, Figure 13 demonstrates that G'' of PtBS348 decreases essentially in proportion to ω and becomes considerably larger than G' while G' decreases more strongly down to $\cong 3 \times 10^6$ Pa on completion of the segmental relaxation, i.e., in the range of ω between the ε'' peak frequency and the crossover frequency toward the Rouse/rubbery behavior. (The dielectric terminal tail, $\varepsilon'' \propto \omega$, is observed at those ω.) This feature, similarly observed also for PI (Figure 12), was helpful for concluding a very minor contribution of the segmental (glassy) relaxation of PtBS to the power-law behavior of the blend modulus at low T seen in Figure 1.

AUTHOR INFORMATION

Corresponding Author
*E-mail: hiroshi@scl.kyoto-u.ac.jp.

ACKNOWLEDGMENT

This work was supported by the Collaborative Research Program of Institute for Chemical Research, Kyoto University (Grant No. 2010-32), Grant-in-Aid for Scientific Research on Priority Area "Soft Matter Physics" from MEXT (Grant No. 18068009), and by Grant-in-Aid for Young Scientists (B) from MEXT (Grant No. 22750204). Q.C. expresses thanks for the support from JSPS.

REFERENCES

(1) Doi, M.; Edwards, S. F. *The Theory of Polymer Dynamics*; Clarendon: Oxford, U.K., 1986.
(2) Watanabe, H. *Prog. Polym. Sci.* **1999**, *24*, 1253–1403.
(3) McLeish, T. C. B. *Adv. Phys.* **2002**, *51*, 1379–1527.
(4) Rubinstein, M.; Colby, R. H. *Polymer Physics*; Oxford: , New York, 2003.
(5) Graessley, W. W. *Polymeric Liquids and Networks: Dynamics and Rheology*; Garland Science: New York, 2008.
(6) Lodge, T. P.; McLeish, T. C. B. *Macromolecules* **2000**, *33*, 5278–5284.
(7) Zetsche, A.; Fischer, E. W. *Acta Polym.* **1994**, *45*, 168–175.
(8) Miller, J. B.; McGrath, K. J.; Roland, C. M.; Trask, C. A.; Garroway, A. N. *Macromolecules* **1990**, *23*, 4543–4547.
(9) Chung, G. C.; Kornfield, J. A.; Smith, S. D. *Macromolecules* **1994**, *27*, 964–973.
(10) Alegria, A.; Colmenero, J.; Ngai, K. L.; Roland, C. M. *Macromolecules* **1994**, *27*, 4486–4492.
(11) Kumar, S. K.; Colby, R. H.; Anastasiadis, S. H.; Fytas, G. *J. Chem. Phys.* **1996**, *105*, 3777–3788.
(12) Wetton, R. E.; Macknight, W. J.; Fried, J. R.; Karasz, F. E. *Macromolecules* **1978**, *11*, 158–165.
(13) Liang, K. M.; Banhegyi, G.; Karasz, F. E.; Macknight, W. J. *J. Polym. Sci., Part B: Polym. Phys.* **1991**, *29*, 649–657.
(14) Miura, N.; MacKnight, W. J.; Matsuoka, S.; Karasz, F. E. *Polymer* **2001**, *42*, 6129–6140.
(15) He, Y. Y.; Lutz, T. R.; Ediger, M. D. *Macromolecules* **2003**, *36*, 8040–8048.
(16) He, Y. Y.; Lutz, T. R.; Ediger, M. D. *Macromolecules* **2004**, *37*, 9889–9898.
(17) Zhao, J. S.; Ediger, M. D.; Sun, Y.; Yu, L. *Macromolecules* **2009**, *42*, 6777–6783.
(18) Angell, C. A. *J. Phys. Chem. Solids* **1988**, *49*, 863–971.
(19) Hodge, I. M. *J. Non-Cryst. Solids* **1996**, *202*, 164–172.
(20) Roland, C. M.; Ngai, K. N. *J. Non-Cryst. Solids* **1997**, *212*, 74–76.
(21) Hirose, Y.; Urakawa, O.; Adachi, K. *Macromolecules* **2003**, *36*, 3699–3708.
(22) Urakawa, O. *Nihon Reoroji Gakkaishi (J. Soc. Rheol. Jpn.)* **2004**, *32*, 265–270.
(23) Watanabe, H.; Urakawa, O. *Korean-Austr. Rheol. J.* **2009**, *21*, 235–244.
(24) Pathak, J. A.; Colby, R. H.; Floudas, G.; Jerome, R. *Macromolecules* **1999**, *32*, 2553–2561.
(25) Pathak, J. A.; Colby, R. H.; Kamath, S. Y.; Kumar, S. K.; Stadler, R. *Macromolecules* **1998**, *31*, 8988–8997.
(26) Pathak, J. A.; Kumar, S. K.; Colby, R. H. *Macromolecules* **2004**, *37*, 6994–7000.
(27) Haley, J. C.; Lodge, T. P.; He, Y. Y.; Ediger, M. D.; von Meerwall, E. D.; Mijovic, J. *Macromolecules* **2003**, *36*, 6142–6151.
(28) Haley, J. C.; Lodge, T. P. *J. Rheol.* **2004**, *48*, 463–486.
(29) Haley, J. C.; Lodge, T. P. *J. Rheol.* **2005**, *49*, 1227–1302.
(30) Watanabe, H.; Ishida, S.; Matsumiya, Y.; Inoue, T. *Macromolecules* **2004**, *37*, 1937–1951.
(31) Watanabe, H.; Ishida, S.; Matsumiya, Y.; Inoue, T. *Macromolecules* **2004**, *37*, 6619–6631.
(32) Watanabe, H.; Sawada, T.; Matsumiya, Y. *Macromolecules* **2006**, *39*, 2553–2561.
(33) Qiao, X.; Sawada, T.; Matsumiya, Y.; Watanabe, H. *Macromolecules* **2006**, *39*, 7333–7341.
(34) Watanabe, H. *Polymer J* **2009**, *41*, 929–950.
(35) Yurekli, K.; Krishnamoorti, R. *J. Polym. Sci., Part B: Polym. Phys.* **2004**, *42*, 3204–3217.
(36) Watanabe, H.; Matsumiya, Y.; Takada, J.; Sasaki, H.; Matsushima, Y.; Kuriyama, A.; Inoue, T.; Ahn, K. H.; Yu, W.; Krishnamoorti, R. *Macromolecules* **2007**, *40*, 5389–5399.
(37) Takada, J.; Sasaki, H.; Matsushima, Y.; Kuriyama, A.; Matsumiya, Y.; Watanabe, H.; Ahn, K. H.; Yu, W. *Nihon Reoroji Gakkaishi (J. Soc. Rheol. Jpn.)* **2008**, *36*, 35–42.
(38) Chen, Q.; Matsushima, Y.; Masubuchi, Y.; Watanabe, H.; Inoue, T. *Macromolecules* **2008**, *41*, 8694–8711.
(39) Fetters, L. J.; Lohse, D. J.; Colby, R. H. *Chain Dimensions and Entanglement Spacings*. In *Physical Properties of Polymers Handbook*, 2nd ed.; Mark, J. E., Ed.; Springer: New York, 2007; Chapter 25, pp 445−452.
(40) Watanabe, H. *Macromol. Rapid Commun.* **2001**, *22*, 127–175.
(41) Chen, Q.; Uno, A.; Matsumiya, Y.; Watanabe, H. *Nihon Reoroji Gakkaishi (J. Soc. Rheol. Jpn.)* **2010**, *38*, 187–193.
(42) T. Sawada, T.; Qiao, X.; Watanabe, H. *Nihon Reoroji Gakkaishi (J. Soc. Rheol. Jpn.)* **2007**, *35*, 11–20.
(43) Inoue, T. *Nihon Reoroji Gakkaishi (J. Soc. Rheol. Jpn.)* **2009**, *37*, 205–210.
(44) Inoue, T.; Okamoto., H.; Osaki, K. *Macromolecules* **1991**, *24*, 5670–5675.
(45) Okamoto, H.; Inoue, T.; Osaki, K. *J. Polym. Sci., Part B: Polym. Phys.* **1995**, *33*, 417–424.
(46) Inoue, T.; Matsui, H.; Osaki, K. *Rheol. Acta* **1997**, *36*, 239–244.
(47) Within the context of the tube model, the PI relaxation in the blends at high T occurs in the fixed entanglement mesh formed by the slow PtBS chains as well as by the PI chains themselves.
(48) Fetters, L. J.; Lohse, D. J.; Richter, D.; Witten, T. A.; Zirkel, A. *Macromolecules* **1994**, *27*, 4639–4647.
(49) Fetters, L. J.; Lohse, D. J.; Graessley, W. W. *J. Polym. Sci., Part B: Polym. Phys.* **1999**, *37*, 1023–1033.
(50) (a) The Kuhn molecular weight of PtBS, $M_{K,PtBS} \cong 1500$, was evaluated from the data for the characteristic ratio ($C_\infty = 13.0 \pm 0.7$)[50b]

and a ratio of the mean-square end-to-end distance to molecular weight reported for PtBS,[39] = $\langle R_{PtBS}^2\rangle/nm^2 = 3.6_1\times10^{-3}M_{PtBS}$. (b) Mays, J. W.; Ferry, W. M.; Hadjichristidis, N.; Funk, W. G.; Fetters, L. J. *Polymer* **1986**, *27*, 129–132.

(51) Kornfield, J. A.; Fuller, G. G.; Pearson, D. S. *Macromolecules* **1989**, *22*, 1334–1345.

(52) Ylitalo, C. M.; Kornfield, J. A.; Fuller, G. G.; Pearson., D. S. *Macromolecules* **1991**, *24*, 749–758.

(53) Ylitalo, C. M.; Fuller, G. G. *Macromolecules* **1991**, *24*, 5736–5737.

(54) Ekanayake, P.; Menge, H.; Ries, M. E.; Brereton, M. G. *Macromolecules* **2002**, *35*, 4343–4346.

(55) Zawada, J. A.; Fuller, G. G.; Colby, R. H.; Fetters, L. J.; Roovers, J. *Macromolecules* **1994**, *27*, 6851–6860.

(56) Zawada, J. A.; Fuller, G. G.; Colby, R. H.; Fetters, L. J.; Roovers, J. *Macromolecules* **1994**, *27*, 6861–6870.

(57) Arendt, B. H.; Krishnamoorti, R.; Kornfield, J. A.; Smith, S. D. *Macromolecules* **1997**, *30*, 1127–1137.

(58) Watanabe, H.; Kotaka, T.; Tirrell, M. *Macromolecules* **1991**, *24*, 201–208.

(59) Doi, M.; Watanabe, H. *Macromolecules* **1991**, *24*, 740–744.

(60) Osaki, K.; Inoue, T.; Uematsu, T.; Yamashita, Y. *J. Polym. Sci., Part B: Polym. Phys.* **2001**, *39*, 1704–1712.

(61) Graessley, W. W. *Adv. Polym. Sci.* **1982**, *47*, 67–117.

(62) We also modified the model (eqs 12a and 13a) by incorporating a minor contribution from the segmental (glassy) relaxation. The resulting model prediction remained very close to that shown in Figure 9 (solid curves).

(63) We also attempted the rheo-optical analysis by incorporating the segmental (glassy) contribution in eq 9. The resulting component moduli were hardly different from those shown in Figure 10, parts b and c (symbols).

(64) Doxastakis, M.; Chrissopoulou, K.; Aouadi, A.; Frick, B.; Lodge, T. P.; Fytas, G. *J. Chem. Phys.* **2002**, *116*, 4707–4714.

(65) The $G_{PI}^{bulk*}(\omega)$ data of the previously examined low-*M* PI ($M = 20\times10^3$)[36,38] did not exhibit a distinct entanglement plateau and were rather close to the data expected for Rouse chains. Thus, the PtBS modulus in the low-*M* PI/PtBS blends[36,38] was successfully evaluated by subtracting the $G_{PI}^{bulk*}(\omega\lambda)$ data from the $G^*(\omega)$ data of the blends not only for the case of the rapid Rouse equilibration ($\tau_e^{PI} \gg \tau_a$) but also for the case of retarded equilibration ($\tau_e^{PI} \le \tau_a$): For the latter case, the Rouse-like mode distribution of $G_{PI}^{bld*}(\omega)$ (eq 12) was close to that of the $G_{PI}^{bulk*}(\omega\lambda)$ data of low-*M* PI so that the subtraction of the $G_{PI}^{bulk*}(\omega\lambda)$ data turned out to be almost equivalent to the subtraction of $G_{PI}^{bld*}(\omega)$.